Optical Materials: X 13 (2022) 100116

Contents lists available at ScienceDirect

Optical Materials: X

journal homepage: www.journals.elsevier.com/optical-materials-x

Invited Article

Linear and nonlinear optical properties of dewetted SiGe islands

Luca Fagiani [a,b], Nicoletta Granchi [c], Attilio Zilli [a], Chiara Barri [a,b], Francesco Rusconi [a], Michele Montanari [c], Erfan Mafakheri [b], Michele Celebrano [a], Mohammed Bouabdellaoui [d], Marco Abbarchi [d], Francesca Intonti [c], Anjam Khursheed [e], Paolo Biagioni [a], Marco Finazzi [a], Maria Antonietta Vincenti [f], Monica Bollani [b,*]

[a] Department of Physics, Politecnico di Milano, Milan, Italy
[b] Institute of Photonic and Nanotechnology - Consiglio Nazionale delle Ricerche, LNESS Laboratory, Como, Italy
[c] LENS and Department of Physics and Astronomy, University of Florence, Sesto Fiorentino, Italy
[d] Aix Marseille Univ, Université de Toulon, CNRS, IM2NP, Marseille, France
[e] Department of Electrical and Computer Engineering, National University of Singapore, Singapore
[f] Department of Information Engineering, University of Brescia, Brescia, Italy

ARTICLE INFO

Keywords:
Solid state dewetting
SiGe nanostructures
Mie resonator
Third- harmonic generation

ABSTRACT

We propose to exploit the natural mechanical instability of thin solid films to form regular patterns of mono-crystalline atomically smooth silicon and germanium nanostructures that cannot be realized with conventional methods. The solid-state dewetting dynamics is guided by pre-patterning the sample by a combination of electron-beam lithography and reactive-ion etching, obtaining precise control over number, size, shape, and relative position of the final $Si_{1-x}Ge_x$ structures. Here we describe our progress in the spectroscopic investigation of individual dewetted $Si_{1-x}Ge_x$ nanoislands: in the linear regime, bright Mie-type localized resonances are detected in the visible spectral range, with a spectral position that can be tuned by modifying the size of the nanoparticles. In the non-linear regime, instead, sizable third-harmonic generation is observed at the level of single islands. We believe that these results will be pivotal to a novel approach in spectral filtering, sensing and structural color with all-dielectric photonic devices.

1. Introduction

Solid state dewetting has been investigated in the last 50 years, being thin film stability a very relevant issue for polymers, metals, and semiconductors [1,2]. In analogy with liquid films breaking into tiny droplets, soft matter and solid films are unstable and break into islands when annealed at temperatures well below their melting point. The thermally activated surface adatom diffusion together with the intrinsic defectivity of the thin layer lead to local thinning of the layer, bringing its top surface in contact with the substrate. At this point, around these heterogeneously distributed holes, a rim forms (where mass accumulates) and starts receding with a speed proportional to the Laplacian of the surface curvature [3–5]. While the rim moves, the underlying Rayleigh-like instability emerges, leading to the formation of fingers that eventually break into islands [5]. The average size and relative distance between the islands are set by the initial layer thickness, by the annealing temperature, and by the interaction with the underlying substrate [6]. For instance, islands of ~100 nm diameter spaced by a few hundred nm can be formed starting from a 30 nm-thick $Si_{1-x}Ge_x$ layer on a 12 nm Si film on SiO_2 [7]. When practical applications are concerned, a templated dewetting approach is the key to tune size and density of the islands, overcoming the randomness of a phenomenon that is intrinsically stochastic [2] or that exhibits correlated disorder when strained bilayers are considered [8,9]. Ordered arrays of individual islands can be obtained in $Si_{1-x}Ge_x$ alloys by patterning the thin layer before annealing by focused ion beam, electron-beam lithography and reactive ion etching, or optical lithography and plasma etching [10–12]. Complex nano-architectures as well as mm-long nanowires and interconnected circuits have been demonstrated and exploited as electronic devices such as field-effect transistors exhibiting state-of-the-art performances [13] and a high level of organization over large arrays [14]. These results are achieved thanks to the mono-crystalline nature of thin silicon on insulator substrates, leading to a precisely controlled dewetting of monocrystalline structures featuring atomically smooth, faceted

* Corresponding author.
E-mail address: monica.bollani@ifn.cnr.it (M. Bollani).

https://doi.org/10.1016/j.omx.2021.100116
Received 18 October 2021; Received in revised form 5 November 2021; Accepted 7 November 2021
Available online 1 December 2021

interfaces that are hardly obtained with other conventional etching methods that typically introduce surface roughness. An interesting application of these dewetted ordered structures is their use as isolated semiconductor emitters. A fully Si-based light source, however, is extremely inefficient because of the indirect bandgap of Si. By introducing ad-hoc emitting impurities, a suitable alternative path to integrate light sources on indirect semiconductor can be used to achieve new photonic devices on silicon [15–17]. Here we present an advancement of a recently emerged approach employing Mie resonators, based on the development of sub-wavelength dewetted $Si_{1-x}Ge_x$ islands with different compositions and dimensions. A key advantage of these resonators is the possibility to obtain resonances spanning the visible and near-infrared range by tuning the original $Si_{1-x}Ge_x$ alloy composition and film thickness. The combination of low losses and high permittivity, along with the very small modal volume [18], makes them ideal candidates for enhancing light–matter interaction and manipulating light at the nanoscale, with a potential to enrich the current performances of photonic devices. High-refractive index nanoantennas based on semiconductors such as silicon [19–21] and germanium [22–24], as well as semiconducting alloys such as aluminum gallium arsenide [25] fabricated using standard lithographic approaches, have been already used as platforms for enhancing nonlinear processes, and in particular third-harmonic generation (THG). Here, along with a thorough optical characterizations by dark field microspectroscopy, we carry out THG measurements on ordered arrays of $Si_{1-x}Ge_x$ -based dewetted nanoislands. Leveraging the large third-order bulk susceptibility of silicon ($\chi^{(3)} = 3.5 \times 10^{-18}$ m^2/V^2 [19]) a sizeable THG is observed at the level of a single dewetted island. Our optical characterizations indicate that the integration of dielectric Mie resonators with light emitters might enable an efficient control of light–matter interaction, therefore favouring the light collection with conventional optics.

2. Materials

We fabricate arrays of thin $Si_{1-x}Ge_x$ islands using a hybrid top-down/bottom-up approach based on the natural morphological evolution of thin solid films under annealing. Specifically, we tested the stability against annealing of two different $Si_{1-x}Ge_x$ alloys: i) 20 nm -thick films of $Si_{1-x}Ge_x$ ($x = 20\%$) and ii) 30 nm-thick films of $Si_{1-x}Ge_x$ ($x = 30\%$) films; both samples are deposited on 12 nm-thick ultra-thin silicon on insulator by molecular-beam epitaxy (MBE) at 500 °C in a static ultra-high vacuum (pressure $\sim 10^{-10}$ Torr). The thickness of the SiO_2 buried oxide (BOX) is 25 nm for both samples. After epitaxial deposition, the $Si_{1-x}Ge_x$ films are patterned by electron-beam lithography (EBL) and reactive-ion etching (RIE) in squares (with sides ranging from 500 nm up to 1 μm) with a pitch between 1 μm and 5 μm [Fig. 1(a) and (b)] [6,13,14]. After etching, the samples are cleaned by oxygen plasma for 20 min and then immersed in a 5% in vol HF solution for 5 s to eliminate any organic contamination and oxide layer. Then, the samples are annealed at high temperatures in the 600 °C–700 °C range in the ultra-high vacuum of a MBE reactor. By atomic force microscopy, at the end of the dewetting process, the island's height is found to vary from about 40 nm for the smaller islands to about 80 nm for the larger ones; while, the final $Si_{1-x}Ge_x$ islands have a lateral size from 150 nm to 550 nm, which is much smaller than the initial patches etched by EBL & RIE, and are electrically isolated from the substrate by the SiO_2 BOX. Dark-field (DF) imaging [Fig. 1(c)] is performed on the $Si_{80}Ge_{20}$ structures by shining white light at ~70° with respect to the sample normal. The diffused light is collected through a high-numerical aperture (NA = 0.75) 100 × magnification objective and imaged onto a colour CMOS camera, using a commercial optical microscope. As the collection angle of the objective lens is smaller than 70°, only scattered light is detected whereas the direct reflection off the sample is rejected, and thus flat surfaces appear black (Fig. 1 (c)). The morphologies of individual dewetted $Si_{1-x}Ge_x$ structures are systematically characterized by scanning electron

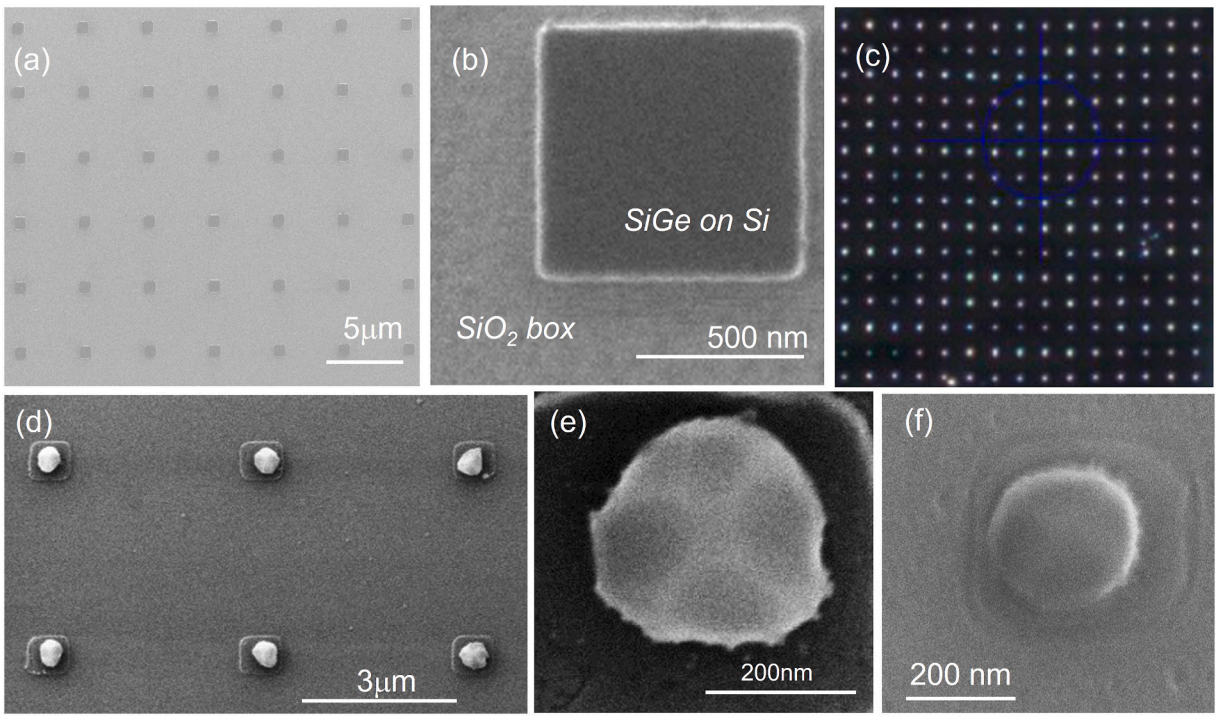

Fig. 1. Planar view electron and optical micrographs of the patterned samples before and after annealing treatments. (a): scheme of the patterned array: $Si_{1-x}Ge_x$ squares with different width and periodicity are created by EBL and RIE etching in a 12 nm-thick ultra-thin silicon on insulator (BOX (SiO_2, 25 nm). (b) High-resolution SEM image of a single $Si_{1-x}Ge_x$ square before the dewetting process. (c) Optical DF image of a 65 × 65 μm^2 typical array of organized dewetted $Si_{80}Ge_{20}$ islands. (d) $Si_{80}Ge_{20}$ dewetted islands obtained after annealing at 650 °C for 1 h; (e) and (f) high-resolution SEM images of individual $Si_{80}Ge_{20}$ (e) and $Si_{70}Ge_{30}$ (f) dewetted islands, showing the equilibrium facets of $Si_{1-x}Ge_x$.

microscopy (SEM) as reported in Fig. 1(d–f). The square area visible under the $Si_{1-x}Ge_x$ island in the SEM images of panels (d) and (f) is due to an imperfect RIE etching of the $Si_{1-x}Ge_x$/Si films before the annealing treatment: during the RIE process, a thin layer of the BOX is etched away, resulting in a step that is not affected by the dewetting instability.

3. Results and discussion

3.1. Dark-field micro-spectroscopy

The fabricated $Si_{1-x}Ge_x$ nano-islands are expected to support Mie-type localized resonances in the visible range, whose spectral position depends sensitively on the island size. In order to assess the linear optical response of the $Si_{1-x}Ge_x$ dewetted islands, we performed DF spectroscopy collecting the scattered signal from single nano-antennas. At variance with the optical dark field image reported in Fig. 1(c), here a different custom-built experimental set-up was implemented on a customized commercial optical microscope as schematized in Fig. 2(a). To achieve the DF regime, a supercontinuum laser is loosely focused with an achromatic lens on the sample surface. The excitation source is tilted by an angle $\theta \approx 30°$ with respect to the axis normal to the sample, larger than the collection angle (given by the numerical aperture NA = 0.45 of the objective). This arrangement ensures that the objective collects only the light scattered by the sample, which is then focused on a multimode optical fiber. At the other end of the fiber the scattered signal is extracted with a reflective collimator and then focused on the entrance slit of a spectrometer where it is dispersed and finally detected by a liquid nitrogen-cooled CCD. The setup allows one to investigate the scattering properties of $Si_{1-x}Ge_x$ dewetted islands in a wide spectral interval (430 nm–850 nm).

Fig. 2 (b) reports the normalized DF spectra of two representative $Si_{80}Ge_{20}$ dewetted islands with diameter of 330 nm and 530 nm, positioned atop a SiO_2 layer of thickness $t = 25$ nm and a semi-infinite Si-bulk substrate The spectra are normalized to the supercontinuum source scattered by a Lambertian surface (Spectralon). The collected spectra exhibit several resonances, the most intense ones observed around 650 nm and 730 nm for the islands with $d = 330$ nm and $d = 530$ nm, respectively, confirming that the resonance shift to longer wavelengths for increasing diameter. It is possible, indeed, to observe a red shift of the spectral features as the diameter increases, while higher order multipolar modes appear [12]. We can conclude that the presented fabrication technique can provide arrays of monocrystalline $Si_{1-x}Ge_x$ islands featuring bright Mie scattering in the visible spectral range, that can be spectrally tuned upon size control of the dewetted islands, which, in turn, is directly correlated with the dimensions of the squares initially patterned by EBL and RIE.

3.2. Nonlinear optical characterization

Nonlinear optical processes can be used to generate light at a frequency multiple of the impinging one. For instance, the input frequency can be tripled via THG. Over the last two decades, much effort was aimed at translating to the nanoscale such harmonic generation capabilities [26]. In subwavelength systems, the intrinsic weakness of nonlinear interactions is compounded by the small volume of matter involved. To make up for this drawback, one can exploit the electromagnetic resonances sustained by subwavelength structures, leveraging on the increased field density to enhance the efficiency of the harmonic generation [27]. Here, we show that, despite the dewetted nanoparticles have more irregular shapes with respect to those produced by the common lithographic techniques (e.g. EBL), sizable third-harmonic (TH) emission can be nonetheless observed at the level of a single dewetted island. Our experimental nonlinear optical characterization is summarized by Fig. 3.

To assess the THG from the dewetted sample we employ a home-made confocal microscope coupled to a pump laser delivering ultrafast (duration $\tau = 160$ fs) pulses at telecom wavelength ($\lambda = 1551$ nm) with a repetition rate $\nu = 80$ MHz. The experimental setup is the same used for similar Si-based metasurfaces and thoroughly described in Refs. [28,29]. In brief, the pump laser is focused on the sample through a 0.85 numerical aperture objective to a diffraction-limited (~1.5 μm diameter) spot. The nonlinear emission by the nanostructures is collected through the same objective in a backscattering configuration and chromatically filtered (centre wavelength/bandwidth in nm: 520/40) to detect the TH emission at 517 nm and reject scattered laser light and (multiphoton) luminescence. High-sensitivity, single-channel detection is performed by a silicon single-photon avalanche diode (SPAD), whose small active region acts as a pinhole, effectively implementing a confocal detection

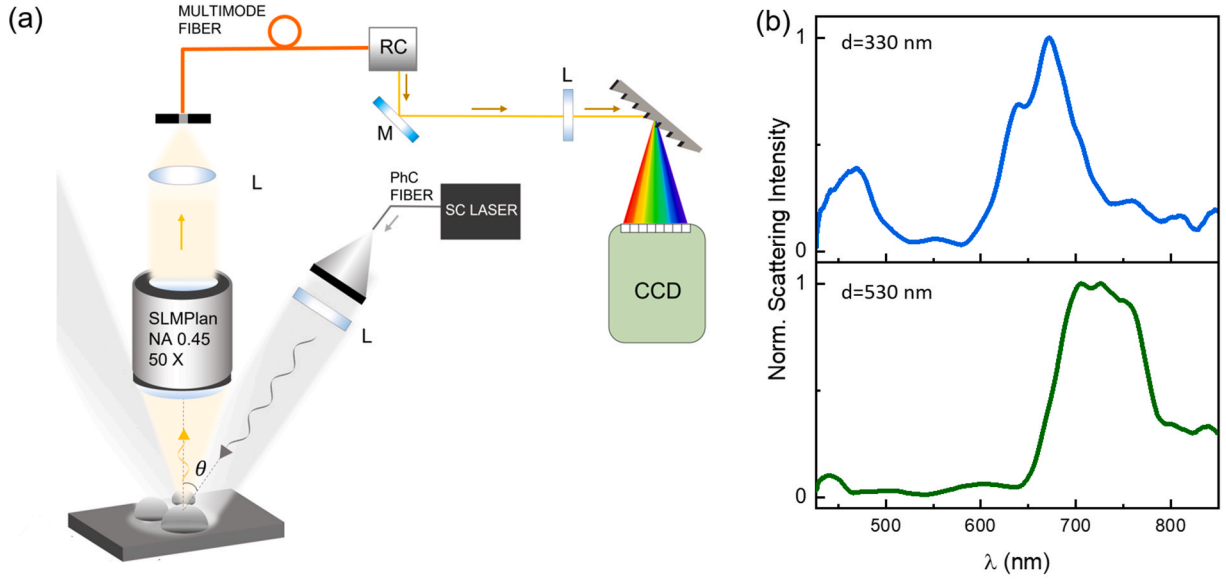

Fig. 2. DF micro-spectroscopy characterization of dewetted $Si_{80}Ge_{20}$ islands. (a) Sketch of the DF setup. (b) Normalized DF spectra of $Si_{80}Ge_{20}$ dewetted island with d = 330 nm (above) and d = 530 nm (below).

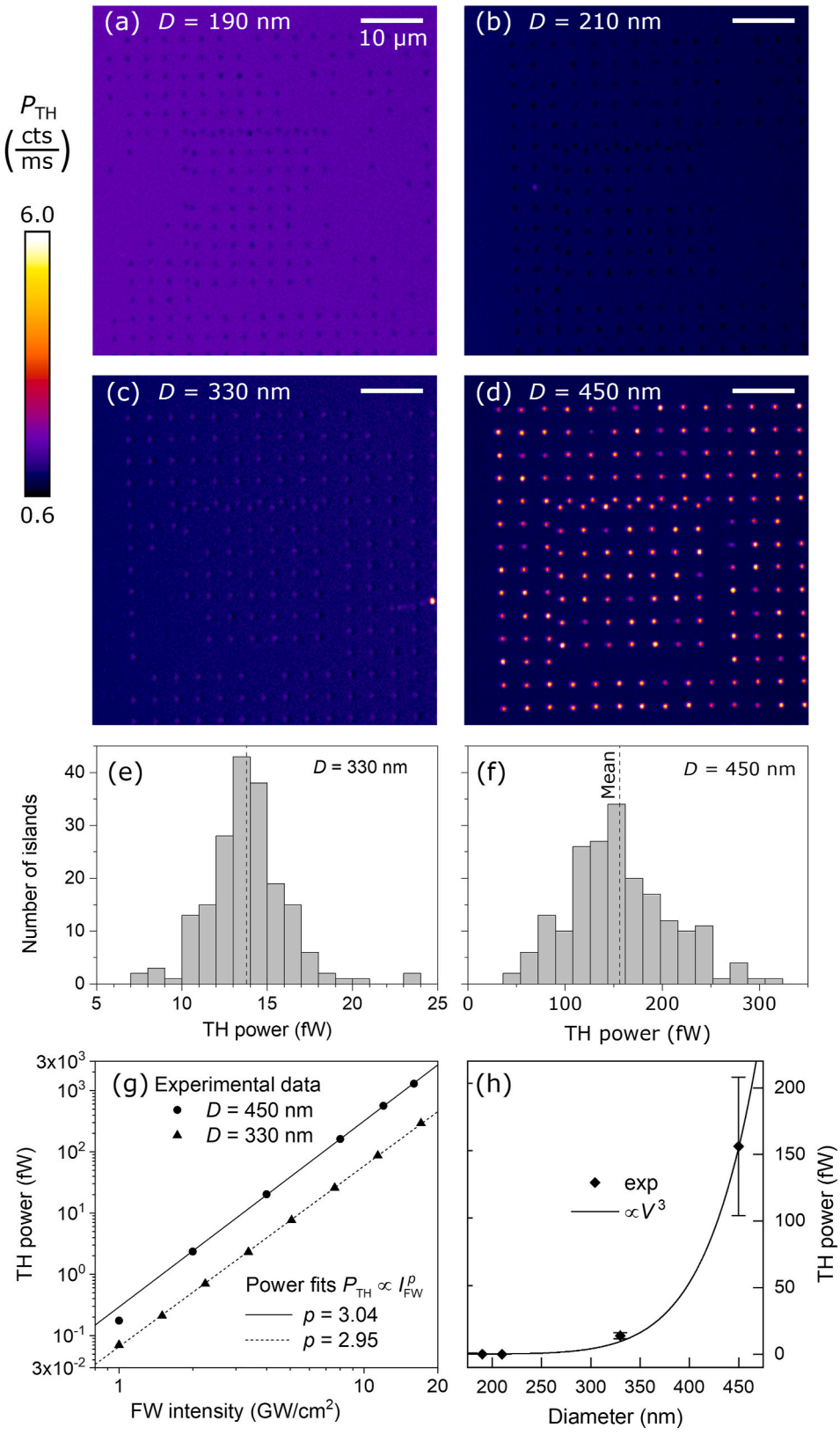

Fig. 3. (a–d). Confocal THG maps in false colors of arrays of dewetted islands of the same nominal diameter d, increasing from (a) to (d). These maps were acquired under an exciting (pulse peak) pump intensity, I_{pk}, *of* 10 GW/cm^2. The common color scale to the left is the time-averaged third-harmonic power, P_{TH}, given in counts/ms. (e,f) Number distribution of the TH emission by the individual islands visible in the maps (c) and (d), respectively. The power is measured from the most intense pixel of each island's raster image, which corresponds to the best centering of the laser spot onto the island. The pixels' grey value is quantified into a power by taking into account the efficiency of the whole detection path and of the detector. (g) Dependence on I_{pk} of the time-averaged TH power emitted by individual islands of different diameter. The symbols are experimental data and the lines are power fits. (h) Dependence of the TH power on the size of the islands. The experimental points are the mean values – highlighted by dashed lines in the histograms (e,f) – whereas the error bars are their standard deviations. The line is an analytical function f(d)∝ d^9 ∝ V^3.

scheme. A piezoelectric sample holder allows raster scanning the sample under the laser spot to produce emission maps such as those displayed in Fig. 3(a–d).

Individual islands, ordered in a square array, can be clearly identified in all maps along with a sizable nonlinear background most likely due to THG or multiphoton-excited luminescence from the underlying Si substrate. However, while TH signal is clearly visible in the maps in Fig. 3(c) and (d), corresponding to the larger islands, smaller islands in the maps a and b instead show a reduced intensity with respect to the background. We tentatively ascribe this result to scattering (either of impinging

radiation or of TH emitted by the substrate) by the island themselves or by the residual EBL square patches – see Fig. 1(d). Some variability between individual islands is visible, most markedly in map (d), which is quantified by the histograms of the TH power distributions reported in panels (e) and (f). The relatively broad distributions reflect the high sensitivity of nonlinear optical processes to the details of the geometry of the emitter, thereby amplifying the sizable morphological dispersity due to the aforementioned stochastic nature of the dewetting process.

Fig. 3(g) displays the dependence of the TH power on the exciting (pulse peak) pump intensity, I_{pk}. The power study was performed on two islands of nominal diameter $d = 450$ nm and $d = 330$ nm. The dependence, spanning over a decade of I_{pk} values, is fitted to a power law (straight lines) and found to be nearly cubic in both cases, which confirms the third-order character of the detected nonlinear signal. For comparison with other platform for harmonic generation at the nanoscale, we quantify the achieved adimensional conversion efficiency as $\eta^{THG} \equiv P_{pk}^{THG}/P_{pk}^{FW}$, where P_{pk}^{THG} is the peak power detected at the TH frequency and P_{pk}^{FW} is the input peak power at the fundamental frequency For instance, the most intense time-averaged THG power ($P_{avg}^{THG} = P_{pk}^{THG}/\tau\nu = 1.3$ pW) reported in panel (g) (obtained for $I_{pk} = 10$ GW/cm^2, namely $P_{avg}^{FW} = 5.3$ mW on the sample) corresponds to $\eta^{THG} = 2.5 \times 10^{-10}$. Another commonly used metric, which has the advantage of being independent from the excitation parameters (pulse peak intensity, duration, and repetition rate) is the nonlinear conversion coefficient $\gamma^{TH} \equiv P_{pk}^{THG}/(P_{pk}^{FW})^3 = 1.4 \times 10^{-15}$ W^{-2}.

Fig. 3(h) shows the emitted TH power as a function of the island diameter. The islands with smaller radii (see maps 3(a) and (b)) yield TH power lower than background level (~1 fW), therefore they are plotted with a null value. Overall, the trend exhibits a steep increase with size, which is explained by the following argument. In the absence of a size-dependent resonant behaviour at the pump wavelength (1550 nm) the electromagnetic energy coupled to the particle is proportional to it volume: $V \propto d^3$, where the height of the droplet is modeled to scale linearly with the diameter d, as inferred from AFM and SEM characterizations. Due to its third-order nonlinear character, the TH power scales with the cube of the in-coupled power, that is, as $P_{pk}^{THG} \propto V^3 \propto d^9$. This analytical dependence, represented by the solid line in panel (h), well reproduces the experimental trend. In the future, by systematic studies of the linear response of the islands their size could be tailored purposefully to enhance the THG through resonances at a given pump wavelength.

4. Conclusions

We showed that solid-state dewetting is extremely well-placed for fabricating sub-micrometric ordered dielectric nano-antennas. We experimentally demonstrated that the nanoislands effectively behave as resonant nanoantennas, whose resonance frequency is governed by size, shape and composition and thus constitutes a precise probe of the dewetted material's homogeneity. In the case of $Si_{80}Ge_{20}$, resonances at ~650 nm and ~730 nm wavelength for the islands with $d = 330$ nm and $d = 530$ nm, respectively, confirm that the Mie resonances shift to the red with increasing dimensions of the scatterers. The nonlinear optical investigation demonstrates that sizeable THG can be achieved upon excitation in the telecom range (1550 nm). Although clear experimental evidence is yet to be provided, the geometry of the islands can be further optimized to favour a resonant enhancement of the THG at visible wavelengths. These linear and nonlinear optical properties make the dewetted $Si_{1-x}Ge_x$ islands a suitable platform for light manipulation at the nanoscale and for integrated semiconductor devices.

Credit authors contribution statement

L. Fagiani., C. Barri, E. Mafakheri. M. Bouabdellaouid, A. Khursheede, M. Abbarchi, M. Bollani conducted the dewetting experiments and microscopical characterizations; N. Granchi, A. Zilli, F. Rusconi, M. Montanari, M. Celebrano, M. Finazzi, P. Biagioni M.A.Vincenti performed linear and nonlinear optical characterizations; M. Abbarchi, F. Intonti, M. Bollani suggested experiments. All authors wrote the manuscript and approved its final version.

Declaration of competing interest

The authors declare that they have no known competing financial interests or personal relationships that could have appeared to influence the work reported in this paper.

Acknowledgements

We acknowledge funding provided by FET-OPEN project NARCISO (no. 828890).

References

[1] D. Quéré, Wetting and roughness, Annu. Rev. Mater. Res. 38 (2008) 71–99.
[2] C.V. Thompson, Solid-state dewetting of thin films, Annu. Rev. Mater. Res. 42 (2012) 399–434.
[3] W.W. Mullins, Theory of thermal grooving, J. Appl. Phys. 28 (1957) 333.
[4] O. Pierre-Louis, A. Chame, Y. Saito, Dewetting of ultrathin solid films, Phys. Rev. Lett. 103 (2009) 195501.
[5] F. Cheynis, E. Bussmann, F. Leroy, T. Passanante, P. Müller, Dewetting dynamics of silicon-on-insulator thin films, Phys. Rev. B 84 (2011) 245439.
[6] M. Abbarchi, M. Naffouti, M. Lodari, M. Salvalaglio, R. Backofen, T. Bottein, A. Voigt, T. David, J.B. Claude, M. Bouabdellaoui, A. Benkouider, I. Fraj, L. Favre, A. Ronda, I. Berbezier, D. Grosso, M. Bollani, Solid-state dewetting of single-crystal silicon on insulator: effect of annealing temperature and patch size, Microelectron. Eng. 190 (2018) 1–6.
[7] A. Benali, J.B. Claude, N. Granchi, S. Checcucci, M. Bouabdellaoui, M. Zazoui, M. Bollani, M. Salvalaglio, J. Wenger, L. Favre, D. Grosso, A. Ronda, I. Berbezier, M. Gurioli, M. Abbarchi, Flexible photonic devices based on dielectric antennas, J. Phys.: Photonics 2 (2020), 015002.
[8] M. Salvalaglio, M. Bouabdellaoui, M. Bollani, A. Benali, L. Favre, J.-B. Claude, J. Wenger, P. de Anna, F. Intonti, A. Voigt, M. Abbarchi, Hyperuniform monocrystalline structures by spinodal solid-state dewetting, Phys. Rev. Lett. 125 (2020) 126101.
[9] Z. Chehadi, M. Bouabdellaoui, M. Modaresialam, T. Bottein, M. Salvalaglio, M. Bollani, D. Grosso, M. Abbarchi, ACS Appl. Mater. Interfaces 13 (31) (2021) 37761–37774.
[10] M. Aouassa, I. Berbezier, L. Favre, A. Ronda, M. Bollani, R. Sordan, A. Delobbe, P. Sudraud, Design of free patterns of nanocrystals with ad hoc features via templated dewetting, Appl. Phys. Lett. 101 (2012), 013117.
[11] M. Abbarchi, M. Naffouti, B. Vial, A. Benkouider, L. Lermusiaux, L. Favre, A. Ronda, S. Bidault, I. Berbezier, N. Bonod, Wafer scale formation of monocrystalline silicon-based Mie resonators via silicon-on-insulator dewetting, ACS Nano 8 (2014) 11181–11190.
[12] N. Granchi, M. Montanari, A. Ristori, M. Khoury, M. Bouabdellaui, C. Barri, L. Fagiani, M. Gurioli, M. Bollani, M. Abbarchi, F. Intonti, Near-field hyperspectral imaging of resonant Mie modes in a dielectric island, APL Photonics 6 (2021) 126102, https://doi.org/10.1063/5.0070626.
[13] M. Bollani, M. Salvalaglio, A. Benali, M. Bouabdellaoui, M. Naffouti, M. Lodari, S. Di Corato, A. Fedorov, A. Voigt, I. Fraj, L. Favre, J.B. Claude, D. Grosso, G. Nicotra, A. Mio, A. Ronda, I. Berbezier, M. Abbarchi, Templated dewetting of single-crystal, ultra-long nano-wires and on-chip silicon circuits, Nat. Commun. 10 (2019) 5632.
[14] M. Naffouti, R. Backofen, M. Salvalaglio, T. Bottein, M. Lodari, A. Voigt, T. David, A. Benkouider, I. Fraj, L. Favre, A. Ronda, I. Berbezier, D. Grosso, M. Abbarchi, M. Bollani, Complex dewetting scenarios of ultrathin silicon films for large-scale nanoarchitectures, Sci. Adv. 3 (2017), eaao1472.
[15] I.A. Khramtsov, A.A. Vyshnevyy, D.Y. Fedyanin, Enhancing the brightness of electrically driven single-photon sources using color centers in silicon carbide, npj Quantum Inf 4 (2018) 15.
[16] W. Redjem, A. Durand, T. Herzig, et al., Single artificial atoms in silicon emitting at telecom wavelengths, Nat. Electron. 3 (2020) 738–743.
[17] D. Toliopoulos, M. Khoury, M. Bouabdellaoui, N. Granchi, J.-B. Claude, A. Benali, I. Berbezier, D. Hannani, A. Ronda, J. Wenger, M. Bollani, M. Gurioli, S. Sanguinetti, F. Intonti, M. Abbarchi, Fabrication of spectrally sharp Si-based dielectric resonators: combining etaloning with Mie resonances, Opt Express 28 (2020) 37734.
[18] I. Staude, A.E. Miroshnichenko, M. Decker, Y. Kivshar, Tailoring directional scattering through magnetic and electric resonances in subwavelength silicon nanodisks, ACS Nano 7 (9) (2013) 7824–7832.
[19] M.R. Shcherbakov, D.N. Neshev, B. Hopkins, A.S. Shorokhov, I. Staude, E.V. Melik-Gaykazyan, Y.S. Kivshar, Enhanced third-harmonic generation in silicon nanoparticles driven by magnetic response, Nano Lett. 14 (11) (2014) 6488–6492.

[20] E.V. Melik-Gaykazyan, M.R. Shcherbakov, A.S. Shorokhov, I. Staude, I. Brener, D. N. Neshev, A.A. Fedyanin, Third-harmonic generation from Mie-type resonances of isolated all-dielectric nanoparticles, Phil. Trans. Math. Phys. Eng. Sci. 375 (2017) 20160281, 2090.
[21] E.V. Melik-Gaykazyan, S.S. Kruk, R. Camacho-Morales, L. Xu, M. Rahmani, K. Zangeneh Kamali, Y.S. Kivshar, Selective third-harmonic generation by structured light in Mie-resonant nanoparticles, ACS Photonics 5 (3) (2017) 728–733.
[22] G. Grinblat, Y. Li, M.P. Nielsen, R.F. Oulton, S.A. Maier, Enhanced third harmonic generation in single germanium nanodisks excited at the anapole mode, Nano Lett. 16 (7) (2016) 4635–4640.
[23] G. Grinblat, Y. Li, M.P. Nielsen, R.F. Oulton, S.A. Maier, Efficient third harmonic generation and nonlinear subwavelength imaging at a higher-order anapole mode in a single germanium nanodisk, ACS Nano 11 (1) (2017) 953–960.
[24] M. Celebrano, M. Baselli, M. Bollani, J. Frigerio, A. Bahgat Shehata, A. Della Frera, P. Biagioni, Emission engineering in germanium nanoresonators, ACS Photonics 2 (1) (2015) 53–59.
[25] A. Zilli, D. Rocco, M. Finazzi, A. Di Francescantonio, L. Duò, C. Gigli, G. Marino, G. Leo, C. De Angelis, M. Celebrano, Frequency tripling via sum-frequency generation at the Nanoscale, ACS Photonics 8 (4) (2021) 1175–1182.
[26] L. Bonacina, P.-F. Brevet, M. Finazzi, M. Celebrano, J. Appl. Phys. 127 (2020) 230901.
[27] D. Smirnova, Y.S. Kivshar, Multipolar nonlinear nanophotonics, Optica 3 (11) (2016) 1241–1255.
[28] L. Fagiani, A. Zilli, A. Tognazzi, E. Mafakheri, K. Okhlopkov, D. Rocco, M. Shcherbakov, A. Fedyanin, C. De Angelis, M. Finazzi, M. Celebrano, M. Bollani, Silicon metasurfaces with tunable electromagnetic resonances for nonlinear optical conversion, Nuovo Cimento C 44 (2021) 4–5, https://doi.org/10.1393/ncc/i2021-21111-9.
[29] A. Tognazzi, K.I. Okhlopkov, A. Zilli, D. Rocco, L. Fagiani, E. Mafakheri, M. Bollani, M. Finazzi, M. Celebrano, M.R. Shcherbakov, A. Fedyanin, C. De Angelis, Third-harmonic light polarization control in magnetically resonant silicon metasurfaces, Opt Express 29 (8) (2021) 11605–11612.